UNCLASSIFIED

SECURITY CLASSIFICATION OF THIS PAGE (When Data Entered)

REPORT DOCUMENTATION PAGE

READ INSTRUCTIONS BEFORE COMPLETING FORM

1. REPORT NUMBER: AFOSR-TR-81-0394
2. GOVT ACCESSION NO.: AD-A098137
3. RECIPIENT'S CATALOG NUMBER:

4. TITLE (and Subtitle): A Model of the Effects of Pressure and Crossflow Velocity on Composite Propellant Burning Rate

5. TYPE OF REPORT & PERIOD COVERED: Interim

6. PERFORMING ORG. REPORT NUMBER:

7. AUTHOR(s): Merrill K. King

8. CONTRACT OR GRANT NUMBER(s): F49620-78-C-0016

9. PERFORMING ORGANIZATION NAME AND ADDRESS:
Atlantic Research Corporation
5390 Cherokee Avenue
Alexandria, VA 22314

10. PROGRAM ELEMENT, PROJECT, TASK AREA & WORK UNIT NUMBERS:
2308A1
61102F

11. CONTROLLING OFFICE NAME AND ADDRESS:
Air Force Office of Scientific Research/NA
Building 410
Bolling AFB, DC 20332

12. REPORT DATE: June 1979

13. NUMBER OF PAGES: 14

14. MONITORING AGENCY NAME & ADDRESS (if different from Controlling Office):

15. SECURITY CLASS. (of this report): Unclassified

15a. DECLASSIFICATION DOWNGRADING SCHEDULE:

16. DISTRIBUTION STATEMENT (of this Report)

Approved for public release; distribution unlimited.

17. DISTRIBUTION STATEMENT (of the abstract entered in Block 20, if different from Report)

APR 2 3 1981

D

A

18. SUPPLEMENTARY NOTES

AIAA/SAE/ASME 15th Joint Propulsion Conference
June 18-20, 1979/ Las Vagas, Nevada

19. KEY WORDS (Continue on reverse side if necessary and identify by block number)

Erosive Burning
Composite Propellants
Propellant Combustion Modeling
Solid Propellant Combustion

20. ABSTRACT (Continue on reverse side if necessary and identify by block number)

Several variations of a model for prediction of burning rate versus pressure behavior of unimodal oxidizer composite propellants in the absence of crossflow were developed and evaluated against a set of data for a series of four formulations. Three variants, including one in which an average oxidizer-burning-surface intersectional area concept is employed and two in which allowance is made for geometry and stoichiometry changes as the

DD FORM 1 JAN 73 1473 EDITION OF 1 NOV 65 IS OBSOLETE

81 4 22 051

UNCLASSIFIED

SECURITY CLASSIFICATION OF THIS PAGE (When Data Entered)

propellant recedes past an oxidizer crystal, were found to give excellent agreement with data. The former variant was extended to treat multimodal oxidizer formulations, yielding predictions in excellent agreement with data for two additional formulations containing bimodal oxidizer. In the initial development of the erosive burning aspect of the model, columnar diffusion flame bending was assumed to be the sole mechanism leading to burning rate augmentation by crossflow; this assumption led to severe underprediction of erosive burning effects. Accordingly, the model was revised through addition of a flow profile analysis for prediction of cross-flow-induced turbulence augmentation of transport properties governing heat feedback from gas flames as well as flame-bending. This revised model was found to yield good agreement with erosive burning data for five of the six formulations tested, but gave higher predicted rates than observed values for the sixth propellant.

SPONSORED BY:
AMERICAN INSTITUTE OF AERONAUTICS AND ASTRONAUTICS (AIAA)
AMERICAN SOCIETY OF MECHANICAL ENGINEERS (ASME)
SOCIETY OF AUTOMOTIVE ENGINEERS (SAE)

A Model of the Effects of Pressure and Crossflow Velocity on Composite Propellant Burning Rate

M. K. King, Atlantic Research Corp., Alexandria, Va.

AIAA/SAE/ASME 15th JOINT PROPULSION CONFERENCE
June 18-20, 1979 / Las Vegas, Nevada

A MODEL OF THE EFFECTS OF PRESSURE AND CROSSFLOW VELOCITY ON COMPOSITE PROPELLANT BURNING RATE*

Dr. Merrill K. King**
Atlantic Research Corporation
Alexandria, Virginia 22314

Abstract

Several variations of a model for prediction of burning rate versus pressure behavior of unimodal oxidizer composite propellants in the absence of crossflow were developed and evaluated against a set of data for a series of four formulations. Three variants, including one in which an average oxidizer-burning-surface intersectional area concept is employed and two in which allowance is made for geometry and stoichiometry changes as the propellant recedes past an oxidizer crystal, were found to give excellent agreement with data. The former variant was extended to treat multimodal oxidizer formulations, yielding predictions in excellent agreement with data for two additional formulations containing bimodal oxidizer. In the initial development of the erosive burning aspect of the model, columnar diffusion flame bending was assumed to be the sole mechanism leading to burning rate augmentation by crossflow: this assumption led to severe underprediction of erosive burning effects. Accordingly, the model was revised through addition of a flow profile analysis for prediction of cross-flow-induced turbulence augmentation of transport properties governing heat feedback from gas flames as well as flame-bending. This revised model was found to yield good agreement with erosive burning data for five of the six formulations tested, but gave higher predicted rates than observed values for the sixth propellant.

Introduction and Background

Erosive burning, the augmentation of solid propellant burning rate by the flow of products across a burning surface, is becoming increasingly important with use of lower port-to-throat area ratio motors and nozzleless motors, both of which result in high velocity crossflows. The response of various propellants to such crossflows must be known by the motor designer in order for him to perform adequate motor design. In addition, it is important that the propellant formulator understand the effect of various formulation parameters on the sensitivity of a propellant to crossflows so that he may tailor his propellants to the desired characteristics. For example, in a nozzleless rocket motor, the decrease in pressure from the head end to the aft end of the grain tends to result in slower burning at the aft end in the absence of erosive effects. Depending upon the sensitivity of the formulation to crossflow, the increasing Mach Number along the grain port may lead to undercompensation, exact cancellation, or over-compensation of the pressure effect. A detailed discussion of the effects of erosive burning on solid propellant rocket interior ballistics for low port-to-throat area ratio motors and nozzleless motors was presented by this author in Reference 1. During the past three years, this author has been conducting an analytical and experimental study of the erosive burning of composite propellants. This effort includes: (1) development of a simplified model for prediction of the erosive burning of a composite propellant, given the non-erosive burning rate versus pressure relationship for that formulation; (2) development of a more fundamental composite propellant combustion model for prediction of burning rate as a function of pressure and crossflow velocity, given only the propellant composition and ingredient particle size distributions; (3) experimental measurement of the erosive burning characteristics (at crossflow velocities up to Mach 1) of a series of propellants with systematically varied compositions and ingredient particle sizes; and (4) fine tuning of the models using this experimental data. The simplified (Generation 1) model has been described in detail in References 2 and 3, with the experimental procedure and test results to date appearing in References 3 and 4.

Details of the first variant of the more fundamental (Generation 2) model for the prediction of burning rate as a function of pressure and crossflow velocity appear in Reference 5. (That reference will be cited heavily throughout this paper, with later variants of the Generation 2 model being described in terms of modifications of the analysis presented therein.) This first variant of the Generation 2 model employs many of the concepts used in the Beckstead-Derr-Price (BDP) composite propellant combustion model[6] with, however, major modifications, including:

1. Variation in the ratio of local oxidizer-surface intersectional area to the binder surface area as the propellant surface regresses past an oxidizer particle is considered. (In the BDP model, a geometrical average ratio is used; this involves an assumption that a lot of very nonlinear processes can be linearly averaged. In tracking the regression of the flame front through an oxidizer crystal in this first model variant, one finds a strong variation in local flame temperature, stoichiometry, and diffusion flame dimensions between polar and equatorial intersections, as discussed in detail in Ref. 5.)

2. The kinetics of subsurface/surface exothermic reactions are considered, with use of rate expressions based upon the work of Waesche and Wenograd.[7] (In the BDP model, subsurface/surface heat release is included with the endothermic ingredient vaporization heats, with the resultant implicit assumption that the amount of heat release in these reactions per unit mass of propellant is independent of such parameters as burning rate.)

3. A correction of an inconsistency in definition of areas in the BDP model is made.

* Research sponsored by the Air Force Office of Scientific Research (AFSC), United States Air Force, under Contract F49620-78-C-0016. The United States Government is authorized to reproduce and distribute reprints for governmental purposes notwithstanding any copyright notation hereon.

** Chief Scientist, Research and Technology Division, Member AIAA

4. The calculation of the dimensionless stoichiometric group needed for calculation of the diffusion flame height via the Burke-Schumann[8] analysis is modified. (The group used in the BDP model is inconsistent with that defined in the original work of Burke-Schumann.)

5. A two-flame (fuel-gas/oxidizer-gas columnar diffusion flame and ammonium perchlorate monopropellant flame), rather than a three-flame model, is used. (With correction of the calculation of the stoichiometry dimensionless group for the Burke-Schumann analysis, it no longer appears necessary to differentiate between the parts of the diffusion flame inside and outside of an ammonium perchlorate monopropellant flame.) (See Figure 1.)

6. The procedure for calculation of heat feedback from the diffusion flame and the AP monopropellant flame is modified. (In the BDP model, all flames are considered to occur in flame sheets at discrete distances from the surface: in the current model, the AP monopropellant heat release is treated as a flame-sheet type heat release but the diffusion flame heat release is considered to occur in a distributed fashion over a finite range of distances from the propellant surface.) (See Fig. 1)

7. The distance (measured normal to the propellant surface) associated with oxidizer-binder gas interdiffusion in the presence of crossflow is assumed to be reduced by a factor, sin θ, where θ is the angle of the resultant of the crossflow and transpiration velocities relative to the surface. (See Figure 1.)

As mentioned earlier, details of the development of the first variant (baseline) of the Generation 2 model are presented in Reference 5. The basic units of the model construction consist of development of a procedure for description of the surface structure at succeeding incremental steps of regression of the binder past an oxidizer particle, application of an energy balance at the surface along with numerous ancillary equations at each increment for calculation of burning rate at that increment, and averaging of the incremental burning mass fluxes to obtain an overall average burning rate. In this baseline varient, an organized crystal array was assumed and used to calculate the relative planar oxidizer and fuel areas at each intersection depth. As discussed in some detail in Ref. 5, choice of the best procedure for calculating an average rate (the "end-game" procedure) is not clear: several averaging equations are presented. The prodedure chosen for use with the first variant of the model was:

$$r_{avg} = \frac{\sum_j (\dot{m}_{ox,p,j} APOX_j + \dot{m}_{fuel,j} AFU_j)}{\rho_{propellant} \sum_j (APOX_j + AFU_j)} \qquad (1)$$

with the summation being carried out over all increments, including ones for which the mass efflux rate is zero. (Since the oxidizer and fuel in general regress at different rates, it is possible for an oxidizer particle to burn out before the binder reaches the bottom of its associated pit, leading to zero burning rate for the remaining increments, as discussed in Ref. 5.)

As explained in detail in References 2 - 5, a mechanism by which crossflow is postulated by this author to affect the burning rate of composite propellants involves the shortening of the distance (measured normal to the surface) associated with the mixing of columns of fuel and oxidizer gas leaving the propellant surface. In the combustion of ammonium perchlorate-loaded composite solid propellants, it is generally accepted that parallel columns of oxidizer and binder sublimation/decomposition product gases leave the surface from above the oxidizer crystals and binder, respectively. In the most general case some heat is fed back to the surface from monopropellant reaction of oxidizer sublimation products while additional heat is supplied by the mixing and reaction of the oxidizer and fuel product streams. (Fig. 1.) Accordingly, an important factor in determining the rate of heat feedback (which increases with decreased distance of the gas-phase heat release zone(s) from the surface) is often the rate of mixing of the oxidizer and binder gas product columns. In the absence of a crossflow, these columns move perpendicular to the propellant surface, while, with crossflow, they are tilted over and travel at an angle to the surface, this angle being determined by the ratio of crossflow velocity to transpiration velocity at any given position above the surface. As a result of this bending, the mixing distance, measured perpendicular to the surface, decreases. A particularly detailed description and explanation of this postulated mechanism is presented in Ref. 3 and 4. In the development of the Generation 1 model and in the early stages of development of the Generation 2 model, this mechanism was assumed to be the only factor causing composite propellant burning rate to increase in the presence of a crossflow.

During the past year, several additional variants of this second-generation model have been developed in a search for an optimum model, both in terms of fundamental physics and in terms of explaining experimental observations regarding the effects of such parameters as pressure, oxidizer particle size, and propellant composition on burning rate. In addition, one of the variants was extended to handle multimodal oxidizer formulations. The original erosive burning section of the Generation 2 model was found to be inadequate, as discussed later, and this section was subsequently modified (in this same variant) to allow for augmentation of gas-phase transport properties by crossflow-generated turbulence as a second erosive burning mechanism. The variants examined are summarized in Table I, and details of the modifications of the original baseline variant (described in detail in Ref. 5) to yield these latter variants are presented in the next section, along with a description of the extension of the selected variant (IV) to handle multimodal oxidizer cases and to treat crossflow-induced turbulent transport property augmentation. Comparison of predictions and data are then presented in the following section.

Model Development

Unimodal Oxidizer, No Crossflow

As indicated above, the first (baseline) variant of the Generation 2 model is described in detail in Reference 5. Nomenclature used in the following model descriptions is consistent with that used in that paper to facilitate comparison. The sole difference between Variant I and Variant II lies in replacement of the procedure of following the receding binder in incremental steps past the oxidizer crystal with use of an "average burning surface-

oxidizer intersection" concept similar to that used by Beckstead, Derr, and Price.[6] (This is, of course, a major simplification to the model since the surface energy balance and ancillary equations described in Ref. 5 need now be solved only once rather than a number of times equal to the number of incremental steps considered in the baseline variant, generally 20 or more. Similarly, the geometric relationships describing the surface only have to be solved once rather than being recalculated sequentially at each increment.) As in the baseline variant, the fuel is assumed to regress in a planar manner and the oxidizer-fuel surface is forced to be continuous at their intersection. These restrictions, coupled with the fact that the linear regression rates of fuel and oxidizer perpendicular to their directions of regression are allowed to differ, force the oxidizer to in general assume a curved shape as it regresses, thus creating additional burning area. As in the BDP model, upper hemisphere and lower hemisphere average intersections are considered and values of the curved oxidizer surface area (ASOX) are calculated at each intersection and averaged together. The "average" intersection in each hemisphere is defined such that the planar oxidizer-burn surface intersectional area (APOX) is the average of the areas of all possible intersections in that hemisphere. With application of geometrical analysis and continuity relationships, it is easily shown that:

$$APOX = \pi D_o^2/6 \tag{2}$$

$$AFU = (\pi D_o^2/6)(1-VLO)/VLO \tag{3}$$

In addition, the distances from the initial top of the oxidizer particle to the fuel surface at the upper and lower intersections can be shown to be

$$XDTOP_{Upper} = (D_o/2)(1 - 1/\sqrt{3}) \tag{4}$$

$$XDTOP_{Lower} = (D_o/2)(1 + 1/\sqrt{3}) \tag{5}$$

Assuming no ignition delay for the oxidizer particle, the corresponding distances from the initial oxidizer peak to the center of the oxidizer crystal at the times when Eqns. 4 and 5 are satisfied are:

$$DELOX_{Upper} = (r_{ox}/r_{fuel})(XDTOP)_{Upper} \tag{6}$$

$$DELOX_{Lower} = (r_{ox}/r_{fuel})(XDTOP)_{Lower} \tag{7}$$

(with restraints that DELOX $\leq D_o$). Again through geometrical arguments, it may be shown that

$$ASOX_{Upper} = \pi(D_o)^2\left[\left(\frac{1}{2} - \frac{1}{2\sqrt{3}}\right)\left(1 - \frac{2\ DELOX_{Upper}}{D_o}\right) + \left(\frac{DELOX_{Upper}}{D_o}\right)^2\right] \tag{8}$$

$$ASOX_{Lower} = \pi(D_o)^2\left[\left(\frac{1}{2} + \frac{1}{2\sqrt{3}}\right)\left(1 - \frac{2\ DELOX_{Lower}}{D_o}\right) + \left(\frac{DELOX_{Lower}}{D_o}\right)^2\right] \tag{9}$$

In Variant II of the second generation model, Eqns. 2 - 9 are used to calculate AFU and ASOX values to replace those used in Variant I. In addition, the increment-dependent flame temperatures and gas heat capacities of Eqns. 32 and 33 in Ref. 5 are replaced by values corresponding to the overall propellant stoichiometry. Finally, the burning rate is calculated as:

$$r_{avg} = \frac{r_{ox}(ASOX)}{APOX} \tag{10}$$

(replacing Eqn. 35 of Ref. 5).

Variant III differs from Variant I in several ways, all of which are believed to entail more realistic descriptions of various processes occurring during the burning of a composite propellant. First, the dependence of the O/F flame kinetic distance, L_{RX}, on the flame temperature was changed from that given by Eqn. 25 in Ref. 5 to:

$$L_{RX} = \frac{K_{OF} V_{gas,surf}(1+\phi)^2 \exp\left[E_{ACT,OF}/RT_f\right]}{p^{(n-1)}\phi} \tag{11}$$

and the corresponding oxidizer flame kinetic distance was altered from Eqn. 26 (Ref. 5) to:

$$L_{AP} = \frac{K_{AP} V_{gas,surf} \exp\left[E_{ACT,AP}/RT_{AP}\right]}{p^{(n-1)}} \tag{12}$$

to allow dependence on local temperature (which is calculated in a trial-and-error loop on the basis of position of the AP flame relative to the beginning and end of the diffusion flame). In addition, the analysis of subsurface heat release was modified to allow reaction only in the liquid melt layer near the surface and to allow for reactant depletion (first order kinetics) with resultant replacement of Eqn. 20 in Ref. 5 by:

$$\alpha = 1 - e^{-ZINT} \tag{13}$$

$$ZINT = \frac{B_{sub}\lambda_{ox} e^{-(E_{sub}/RT_s)} RT_s^2 (1-e^{-U_L E_{sub}(T_s-T_o)/RT_s^2})}{r_{ox}^2 \rho_{ox} C_{pox} E_{sub}(T_s - T_o)} \tag{14}$$

$$\left.\begin{aligned} U_L &= -\ln\frac{T_{melt} - T_o}{T_s - T_o} \quad \text{for } T_s > T_{melt} \\ U_L &= 0 \quad \text{for } T_s \leq T_{melt} \end{aligned}\right\} \tag{15}$$

Finally, the assumption in Variant I that the O/F flame heat release is uniform between $y = L_{RX}$ and $y = L_{RX} + FH90\sin\theta$ was replaced with a distributed heat release more heavily weighted toward the base of the diffusion flame, this weighting determined by detailed mixing profiles calculated via the Burke-Schumann[8] analysis. This resulted in replacement of Eqns. 22 and 23 of Ref. 5 with considerably more complex expressions for heat feedback fluxes from the gas-phase flames.

As indicated in Table I, Variant IV is the same as Variant III except for use of an "average intersection" concept: thus, modification of Variant III to Variant IV follows exactly the same procedure as the modification of Variant I to Variant II, described earlier.

Variants V and VI represent modifications of Variant III to allow different surface temperatures for the binder and oxidizer. To permit this, separate energy balances are written for the oxidizer and binder (replacing Eqn. 34 of Ref. 5), with the oxidizer receiving feedback from the oxidizer monopropellant flame and the diffusion flame, while the binder receives feedback only from the diffusion flame. The diffusion flame feedback is apportioned between binder and oxidizer in the ratio of the planar fuel and oxidizer areas. Subsurface heat release is apportioned so that the oxidizer receives

the fraction, 1/(1 + SMRBO), while the binder receives the fraction SMRBO/(1 + SMRBO), where SMRBO is the stoichiometric ratio (mass) of binder to oxidizer. The only difference between Variants V and VI lies in the treatment of the effect of non-planar surface structure on gas flame standoff distances relative to the oxidizer surface. In Version V, allowance is made for the non-planar structure. For oxidizer protruding, the distance from the oxidizer surface to the outer edge of the O/F flame is reduced by the average protrusion height. For oxidizer recessed, the distance from the oxidizer surface to both the inner and outer edges of the O/F flame is increased by the average recession depth. In Version VI, no such adjustment is made, it being assumed that the flame is wrinkled in such a manner as to track the surface contour.

Variants IIIA, IIIB, and IIIC all represent modifications of Variant III aimed at increasing the predicted dependence of burning rate on overall propellant flame temperature. (As will be discussed later, the strong variation of flame temperature with increment location in Variant III causes the effect of overall average flame temperature to be fairly well washed out in application of that variant.) Variant IIIA is quite similar to Variant III except that instead of using flame temperature (T_f) and gas heat capacity (C_p) values corresponding to the local oxidizer/fuel ratio at each increment (as expressed by Eqns. 32 and 33 in Ref. 5), we use flame temperature and heat capacity values equal to the overall propellant flame temperature and gas heat capacity, independent of increment number, at each increment. That is, Eqns. 32 and 33 of Ref. 5 are replaced by:

$$T_f = f_2\ (WFO/(1-WFO)) \tag{16}$$

$$C_p = f_3\ (WFO/(1-WFO)) \tag{17}$$

where the functionalities are generated by application of a thermochemical equilibrium calculation. Consistent with this modification, we also slightly modify the "end-game" procedure of calculating the overall propellant linear burning rate from the mass flux values calculated at each incremental intersection. Equation 1 of this paper is still employed, but the summations are now limited to incremental intersections for which the mass fluxes are non-zero. (That is, increments corresponding to post-oxidizer-burnout are not considered, with the assumption being made that the residual binder "breaks off" in some manner.) This has no effect on the numerator of Eqn. 1, but lowers the value of the denominator in cases where the oxidizer recedes more rapidly than the binder. (This modification of the "end-game" procedure is consistant with the use of flame temperature equal to overall propellant flame temperature at each incremental intersection in that such use implies an oxidizer/fuel ratio in the final flame equal to the overall propellant oxidizer/fuel ratio, thus implying that the "left over" binder is indeed somehow fed into the flame. It must be emphasized that this is not a closed question, however. As discussed in Ref. 5, definition of an optimum "end-game" procedure for calculation of an average linear propellant regression rate from values calculated at various points in the passing of the burning front through an oxidizer particle is somewhat nebulous, at best.)

Variant IIIB is also a derivative of Variant III, with arbitrary assignment of fuel to oxidizer at various incremental intersections according to:

$$\frac{AFU}{APOX} = C_x\ (DPOX)^{XNA}, \quad -1 \le XNA < 0 \tag{18}$$

where XNA is an arbitrary input constant and C_x is determined for a given value of XNA by consideration of overall continuity for the propellant. A value of XNA = 0 corresponds to the ratio of fuel to oxidizer pl: · intersectional areas being independent of increment number, while XNA<0 results in polar intersections burning more fuel-rich than equatorial intersections. As will be discussed later, this variant showed very little promise for values of XNA between 0 and -1, and was quickly discarded.

In Variant IIIC, still another offshoot of Variant III, the oxidizer/fuel ratio of gas streams associated with a given oxidizer particle at each ntersection depth was forced to be the same, equal to the overall propellant oxidizer/fuel ratio. This was accomplished by adjusting the fuel area associated with the oxidizer at each intersection depth in accordance with:

$$AFU = \frac{(1 - WFO)\ \dot{m}_{ox,p}\ APOX}{(WFO)\ \dot{m}_{fuel}} \tag{19}$$

This modification corresponds to doing away with the concept of an organized matrix of oxidizer crystals in the binder matrix, employed in Variants I, III, V, VI, and IIIA (and described in detail in Ref. 5), and replacing it with the assumption that random distribution of oxidizer crystals results in the average O/F characteristics of a polar intersection (averaged over all polar intersections) and the average O/F characteristics of an equatorial intersection being the same. Among other things, this approach has the pleasing effect of eliminating the problem of "leftover" binder which crops up with the other variants. In addition, the average linear propellant burn rates calculated using the different averaging procedures described in detail in Ref. 5 are more nearly equal in this variant than in the other variants considering incremental passage of the burning surface through an oxidizer particle. Further, as will be discussed later, this variant is much more successful than Variant III in predicting dependency of burn rate on overall propellant oxidizer/fuel ratio (and thus flame temperature). A different means of calculating average burn rate from the individual incremental rates (Eqn. 37 in Ref. 5) was found to give slightly better results than the procedures used in the other model variants. In this procedure, the burning rate is calculated by dividing the oxidizer particle diameter by the sum of the times required for consumption of each incremental thickness until the bottom of the oxidizer particle is reached:

$$r_{avg} = D_o/\Sigma_j\ TAU_j = D_o/\Sigma_j[\Delta(DELOX)_j/r_{ox,j}] \tag{20}$$

To this author, this is another plus point for this variant since Eqn. 20 seems to be more physically realistic than Eqn. 1 for calculation of the average linear regression, though it did not produce satisfactory results in the other variants studied.

Multimodal Oxidizer, No Crossflow

As will be discussed later, Variants IIIA, IIIC, and IV were all found to give satisfactory results when tested against no-crossflow burning rate data for a series of four unimodal oxidizer composite propellants. Although Variant IIIC is the most appealing to this author on a physical basis, the

considerably lower computational complexity associated with Variant IV led to its selection for extension for multimodal oxidizer cases. This extension was carried out in a very straightforward manner using Glick's "petit ensemble" approach[9], in which a propellant containing oxidizer particles of different sizes is broken into a series of subpropellants or "pseudopropellants", each of which contains oxidizer of only one size. These subpropellants are assumed to burn non-interactively, with the unimodal oxidizer model being used to calculate a mass flux for each, and straightforward averaging weighted according to fractional surface areas associated with each subpropellant then being used to obtain an overall propellant average linear regression rate. The only manner in which oxidizer of one size is allowed to affect the burning of a subpropellant containing oxidizer of another size is through possible influence on the assignment of fuel to that subpropellant. That is, rather than fuel being assigned to each oxidizer size category in direct proportion to the amount of oxidizer in that category, the capability of allowing uneven assignment of fuel to various oxidizer size subpropellants is allowed by means of a power law:

$$V_{f,d_i} = C_2 \, (D_o)_i^{XEXP} \tag{21}$$

where V_{f,d_i} is the volume of fuel assigned to a particle of diameter $(D_o)_i$, XEXP is an arbitrary input power law constant, and C_2 is a constant determined by application of overall continuity. It may easily be shown that XEXP = 3 will result in each subpropellant having the same oxidizer/fuel ratio as the overall propellant O/F ratio. XEXP<3, on the other hand, will result in subpropellants with small oxidizer being more fuel-rich than the overall propellant and subpropellants with large oxidizer being more fuel-lean, with the reverse occurring for XEXP>3.

Thus, the modification of Variant IV of the Generation 2 burning rate model to handle multimodal oxidizer cases consists simply of adding a package at the front of the program to define the subpropellants, using the existing program to calculate burning rates for each subpropellant, and properly averaging these rates.† The additional equations employed are (with γ_i being defined as the mass of oxidizer particles of particle diameter $(D_o)_i$ per unit mass of total propellant):

$$\gamma = \Sigma \, \gamma_i \tag{22}$$

$$\rho_{propellant} = 1/[\gamma/\rho_{ox} + (1-\gamma)/\rho_{fuel}] \tag{23}$$

$$C_2 = \frac{\frac{\pi}{6}\left(1 - \frac{1}{1+\rho_{ox}(1-\gamma)/\rho_{fuel}\gamma}\right)\left(\gamma+\rho_{ox}(1-\gamma)/\rho_{fuel}\right)}{\sum_i \left(\gamma_i/(D_o)_i^{3-XEXP}\right)} \tag{24}$$

ζ_i^* = Volume Fraction Oxidizer in Subpropellant i $= 1/[1+6C_2(D_o)_i^{XEXP-3}/\pi]$ (25)

γ_i^* = Mass Fraction Oxidizer in Subpropellant i $= 1/[1+6C_2\rho_f(D_o)_i^{XEXP-3}/\pi\rho_{ox}]$ (26)

ρ_i^* = Density of Subpropellant i $= \rho_{ox}\, \zeta_i^*/\gamma_i^*$ (27)

$$r_{avg} = (1/\rho_{ox}) \, \Sigma_i(\dot{m}_{p,d_i}\gamma_i)/\zeta_i^* \tag{28}$$

†Currently under review

Modification of Erosive Burning Package

Use of the erosive burning package originally built into the different Generation 2 model variants led in all cases, as discussed in the next section, to major underprediction of the effect of crossflow on burning rate, indicating that the proposed flame-bending mechanism was by itself insufficient. Accordingly, a second possible mechanism, augmentation of turbulence transport properties in the region between the propellant surface and the gas-phase flames was invoked and combined with the flame-bending mechanism. In this approach, it was assumed that both the effective thermal conductivity (governing feedback from the various gas flames) and the effective mass diffusivity (an important parameter in determining the thickness of the diffusion flame) were increased in crossflow situations by crossflow-induced turbulence. A flow profile analysis permitting calculation of eddy viscosity (and, by analogy, total effective thermal conductivity and diffusivity) as a function of distance from the propellant surface for a given crossflow velocity, transpiration velocity (determined by the propellant burning rate), and temperature field (dependent on the location of gas-phase heat release zones) was developed and coupled with the Variant IV combustion model for erosive burning calculations. An improved calculation of diffusion flame-bending angle was also incorporated in this analysis.

For this analysis, preliminary estimates of the burning rate (and thus transpiration velocity) and the distance from the surface to the end of the diffusion flame (L_{RX} + FH90 sin θ) were first made using laminar transport properties as in the original erosive burning package. The nonblowing skin friction coefficient was then calculated as the maximum of a value calculated using a smooth-wall equation and one calculated using a rough-wall equation:

$$C_{fo} = .00140 + .125 \, Re^{-0.32} \tag{29}$$

$$C_{fo} = 0.95 \, [4 \log_{10} (R/k) + 3.48]^{-2} \tag{30}$$

A blowing parameter, b:

$$b = \frac{2 \dot{m}_{INJ}}{\rho_{fs} U_{fs} C_{fo}} \tag{31}$$

was then calculated from the previously estimated burning rate and the freestream velocity. This parameter was next used to estimate the actual skin friction coefficient with blowing (transpiration). Unfortunately, there is essentially no data available for values of b greater than 6 - 8, and our range of interest tends to go to much higher blowing ratios. Accordingly, several different expressions were fit to existing data[10-14] and built into the program for optional means of calculating skin friction with blowing:

$$C_f/C_{fo} = \exp\left[-.357\, b + .0068\, b^2\right], \quad b \le 26.25 \tag{32a}$$
$$= .0092, \quad b > 26.25$$

$$C_f/C_{fo} = \exp\left[-.5513 b + .01316\, b^2\right], \quad b \le 20 \tag{32b}$$
$$= .0031, \quad b > 20$$

$$C_f/C_{fo} = \exp(-0.576\, b) \tag{32c}$$

$$C_f/C_{fo} = b/(\exp(b) - 1.0) \tag{32d}$$

Next, the wall shear stress was calculated as:

$$\tau_{wall} = \rho_{fs} u_{fs}^2 (C_f/2) \quad (33)$$

Application of a momentum integral analysis for a two-dimensional channel (the configuration in which testing was conducted) yields the following expression for local shear stress as a function of distance from the propellant surface and local crossflow velocity:

$$\tau = \tau_{wall} + \dot{m}_{INJ} u - Ky \quad (34)$$

$$K = 0.9 \dot{m}_{INJ} \bar{U}_{crossflow} \left[\frac{2+(\gamma_c+1)M^2_{crossflow}}{1-M^2_{crossflow}}\right]/h$$

(It should be noted that the -Ky term in this equation results from the axial pressure gradient term caused by friction and mass injection in a confined channel: this term has not been included in several previous similar analyses of erosive burning. At sufficiently high blowing ratios (leading to low τ_{wall} values) this term can be very important; even, in some cases, causing the calculated shear stress to be negative away from the surface. This author interprets this condition as indicating boundary layer blowoff: when this condition is met, an alternate boundary layer analysis is employed, as discussed later.)

At any rate, application of Eqns. 29-34 permits calculation of local shear stress, τ, as a function of distance from the propellant surface (y) and local crossflow velocity (u) for a given set of free-stream conditions, mass injection rate, and temperature field. [$\tau = g_1(u,y)$]. An eddy viscosity approach is used to relate the local shear stress to the local crossflow velocity gradient via:

$$\tau = (\mu + \rho\epsilon)\, du/dy \quad (35)$$

With specification of an expression for ϵ as a function of y and du/dy (discussed below), and use of:

$$\rho = P(MW)/RT \quad (36)$$

$$\mu = kT^{0.8} \quad (37)$$

$$T = T_s + \frac{(T_f - T_s)y}{L_{RX}+FH90 \sin\theta} \quad (38)$$

(the latter equation resulting from assumption of a linear temperature profile from the surface to the end of the diffusion flame), Eq. 35 may be combined with the $\tau = g_1(u,y)$ relationship obtained from Eqns. 29-34 to yield a first order differential equation for local crossflow velocity. With use of u = 0 at y = 0, this is numerically integrated from the wall to yield u(y), ϵ(y), ρ(y), and μ(y). (In addition, with use of $v(y) = \dot{m}_{INJ}/\rho$, v(y) is obtained and the shape of streamlines emanating from the surface are calculated, permitting calculation of an effective diffusion flame bending angle, θ, allowing for the fact that the bent flame is curved rather than straight, as assumed in the earlier version of the erosive burning package.) These results are used to calculate

$$\lambda_{eff}/\lambda_L = \mathcal{D}_{eff}/\mathcal{D}_L = 1+\rho\epsilon/\mu = g_2(y) \quad (39)$$

That is, the ratio of transport total properties to laminar properties is calculated as a function of distance from the surface. Average total transport property values between appropriate zones are then calculated and substituted for the laminar values in the diffusional mixing equations and the heat feedback equations in the original model, revised burn rates and flame distances are calculated, and the procedure is repeated until convergance is achieved. As might be expected, this looping procedure is considerably more complex in the case of multimodal propellants than for unimodal propellants since solution of the individual subpropellant cases becomes interactive in the case of crossflow. This interaction occurs because there is only one boundary layer for the overall propellant (that is, one cannot calculate a different boundary layer profile for each subpropellant) with the boundary layer details being controlled by the average transpiration velocity, flame height, surface temperature, etc. for the overall propellant rather than by the individual values of these parameters for each subpropellant.

Several options for closure of the boundary layer analysis through use of an eddy viscosity equation were built into the program: all entailed use of a Prandtl mixing-length type expression. The most comprehensive of these was a modified form of an empirical relation developed by Kays and Moffat[11] which includes the effects of blowing and axial pressure gradient but does not include the effects of roughness. The modifications added by this author were an attempt to include the effects of roughness using approaches suggested by the works of van Driest[15] and Cebeci and Chang[16]. The resulting expression is:

$$\epsilon = .168(y+\Delta y)^2 \frac{du}{dy}\left\{1.0-\exp\left[\frac{-(y+\Delta y)u^*\Gamma}{25\nu}\right]+\exp\left[\frac{-2.6(y+\Delta y)\Gamma}{k}\right]\right\}^2$$

$$\epsilon = .168(y+\Delta y)^2 \frac{du}{dy} \text{ for } \frac{ku_*}{\nu} > 65 \quad (40)$$

where:

$$\Delta y = 0.9\frac{\nu}{u_*}\left[\sqrt{\frac{ku_*}{\nu}} - \frac{ku_*}{\nu}\exp\left(\frac{-ku_*}{6\nu}\right)\right] \quad (41)$$

$$\Delta y = 0 \text{ for } \frac{ku_*}{\nu} \leq 4.535$$

$$\Gamma = 1+7.1\left\{\frac{V_{gas,surf}}{u^*} + \frac{4.25\nu\, g_c \frac{dp}{dx}/\rho u_*^3}{1+10V_{gas,surf}/u_*}\right\} \quad (42)$$

The second exponential is Eqn. 40 is included to force the damping function (major brackets) to go to unity as the roughness Reynolds Number (ku^*/ν) approaches 65 (full roughness), consistent with the van Driest[15] approach. The Δy term reflects a profile displacement due to roughness as suggested by Cebeci and Chang[16]. Other options considered included use of the van Driest expression without blowing or pressure gradient effects, use of the above expression with Δy set equal to zero for all roughness values, and use of an expression with no damping (with or without a roughness Δy factor). The expression which thus far seems to give the best results is the no-damping, no-roughness expression:

$$\epsilon = .168\, y^2\, du/dy \quad (43)$$

though it must be admitted that this is not the most pleasing on physical grounds.

As mentioned earlier, depending on the C_f/C_{fo} relationship used there are cases (high blowing parameter ones) where attempts to integrate the shear stress equation out from the surface results in the local shear stress going negative: this is interpreted as representing some type of boundary layer blowoff. In this case, it is assumed that the velocity profile assumes the cosine law shape (inviscid no-wall-slip flow) measured by Yamada and Goto[17] among others, and this profile is then differentiated and the result substituted into Eqn. 43 to yield the eddy viscosity distribution, without

use of momentum equation, though it is realized that this is not a very satisfactory resolution of the problem. A major difficulty with the entire boundary layer analysis outlined above is that the blowing ratio (transpiration velocity/crossflow velocity) values generally encountered in erosive burning are well outside the range for which boundary layer details have been even marginally defined. To quote H. W. Liepmann, "Extrapolation is clearly anything but safe when the methods used rely on experimental confirmation of specific cases rather than a deeper understanding of the fluid dynamics of turbulence": such is the case here.

Comparison of Predictions and Data

A family of six ammonium perchlorate (AP)/hydroxyterminated polybutadiene binder (HTPB) propellant formulations has been used for testing and "tuning" of the Generation 2 burning rate model variants described in the preceding section. Burning rate versus pressure data have been obtained at various crossflow velocities (including zero crossflow) for these formulations, which are listed in Table II. As may be seen, four of the formulations tested contain unimodal oxidizer, while the other two contain bimodal oxidizer. The unimodal formulations cover three particle sizes and two oxidizer/fuel ratios. In each variant of the Generation 2 model, there are three "free" constants which are optimized in terms of the data. These constants are K_{AP}, a pre-exponential in the expression relating the monopropellant flame kinetic delay distance to pressure, temperature, and burning gas velocity (Eq. 12), K_{OF}, a similar pre-exponential for the O/F flame kinetic delay distance expression (Eq. 11), and B_{sub}, a pre-exponential for the subsurface/surface reaction rate expression. The procedure which has been employed in this study is to optimize these constants for each variant against the no-crossflow burn rate data for the unimodal propellants, and then leave them unchanged as a given variant is extended to multimodal propellants and crossflow situations. Now that Variant IV has been extended to handle such cases, reoptimization of the constants against all of the data for the unimodal and multimodal propellants (with and without crossflow) might be considered: at this time, this latter procedure has not been employed.

Unimodal Oxidizer Propellants, No Crossflow

Each of the Generation 2 model variants was tested against no-crossflow data for the unimodal propellants listed in Table II, with optimization of the constants K_{OF}, K_{AP}, and B_{sub}. As a result of this procedure, several variants were eliminated from further consideration. Although Variants I and III appeared to provide comparable agreement with data, Variant I was eliminated because it was felt that the modifications made in going from I to III resulted in a more physically correct model. Similarly, Variant II was eliminated relative to Variant IV.

With Variants III, V, and VI, values of the three free constants could be found which would give excellent agreement with the no-crossflow burn rate versus pressure data for the first three formulations of Table II: however, use of these same constants for the fourth propellant resulted in serious underprediction of the burning rate. The cause of this behavior was tracked down to be a tendency of these models to underemphasize the effect of overall average propellant flame temperature on the burning rate. This tendency resulted from the fact that the averaging procedure (for averaging over the various intersection increments) put a good deal of weight on the burning rates of increments for which the oxidizer/fuel ratio was considerably higher than the overall oxidizer/fuel ratio (near-equatorial intersections). Since the rate of flame temperature increase with increasing O/F ratio decreases as the O/F ratio approaches stoichiometric (all of these formulations are fuel-rich overall) the flame temperature of the near-equatorial intersection increments is nearly the same for the 1667°K formulations (4525, 4685, and 5051) as for the 2065°K formulation (5542). As a result the predicted burning rates for these near-equatorial increments are nearly the same for the two 20 micron oxidizer formulations, with the result that a set of constants which gives good agreement between theory and data for the 1667°K formulations tends to result in underprediction of burn rate for the hotter formulation. It was this result that led to development of Variants IIIA, IIIB, and IIIC, in which more emphasis was placed on insuring that overall formulation flame temperature would have more direct influence on the predicted burning rate.

Variant IIIB was found to give unsatisfactory results for all values of the fuel-assignment parameter (XNA) examined and was consequently dropped. The search for an optimum value of XNA was limited to values between 0 and -1: it may be that a more negative value would result in improvement of agreement between theory and data, but it seemed more worthwhile to pursue Variants IIIA and IIIC since they seemed more attractive on physical grounds (particularly IIIC) and required fitting of one less empirical constant.

Predicted and experimental burn rate versus pressure results for the four unimodal formulations in the absence of crossflow are presented for Variants IIIA, IIIC, and IV in figures 2, 3, and 4, respectively. As may be seen, with optimization of the three free constants (slightly different for the three variants, as might be expected) all three variants permit excellent prediction of the burning rate versus pressure characteristics of the four formulations, Variant IIIA giving the best agreement of theory with data. Since Variant IV did not give appreciably worse results than the other two variants and was considerably simpler to extend to treatment of multimodal oxidizer formulations and to crossflow cases using the erosive burning package described in the previous section, it was selected for first extension to those cases.

Multimodal Oxidizer Propellants, No Crossflow

The extension of Variant IV of the Generation 2 model to handle multimodal oxidizer cases was described in the preceding section. Results of use of this extended model to predict no-crossflow burn rate versus pressure behavior for the two bimodal oxidizer formulations listed in Table II are presented in Figure 5. It should be noted that the values of K_{AP}, K_{OF}, and B_{sub} selected during analysis of the unimodal oxidizer formulations are not changed: that is, they are no longer free constants. The predictions shown in Figure 5 were made with the fuel-assignment constant (XEXP) set equal to 3 (resulting in equal stoichiometry subpropellants).

As may be seen, agreement between theory and data is excellent except at the high pressure end of data for the 90/200 micron formulation (5565). The two highest pressure data points for this formulation appear to roll off severely, while the predicted rates continue to climb. The reason for this behavior is not clear. Limited calculations using lower values of XEXP (corresponding to the small oxidizer size subpropellant being more fuel-rich than the large oxidizer size subpropellant) yielded worse agreement with data.

Erosive Burning Predictions Using Only Flame-Bending

As discussed earlier, all of the model variants examined originally contained an erosive burning package based on the assumption that the sole mechanism causing burning rate increase with crossflow is the bending over of columnar diffusion flames by that flow. (This package is described in detail for Variant I in Ref. 5.) For all variants, with free constants optimized from matching no-crossflow data as described earlier, this assumption led to the underprediction of crossflow effects for all formulations at all pressures and crossflow velocities. An example of this underprediction is shown in Figure 6, where predictions made using Variant IV with the original erosive burning package are compared with data for Formulation 4525 (73/27 AP/HTPB, 20 micron AP). Based on these results, the erosive burning portion of the Generation 2 model was revised as described in the previous section to allow consideration of augmentation of gas transport properties by crossflow-induced turbulence as well as flame bending.

Erosive Burning Data Comparison With Revised Model Predictions

Several different eddy viscosity models and several equations for extrapolation of skin friction data to high blowing ratio conditions were built into the revised Variant IV model, as discussed earlier. Studies to date indicate that the erosive burning data for the formulations listed in Table II are best predicted using the no-damping, no-roughness eddy viscosity expression (Eq. 43) and the first of the four C_f/C_{fo} expressions (Eq. 32a), but a firm conclusion regarding the most suitable expressions has not yet been made. (As indicated, a major difficulty with this analysis is that it involves making boundary layer predictions in a blowing-ratio regime which has not been studied, and extrapolation of turbulent flow field data is extremely risky.) Theoretical predictions and data for the six formulations tested to date are presented in Figures 7 - 12. As may be seen, the agreement between theory and data for five of the six formulations is quite encouraging. With Formulation 5565 (the 82/18 AP/HTPB bimodal formulation with 90 and 200 micron ammonium perchlorate) however, the model predicts considerably more sensitivity of burning rate to crossflow than actually observed. Use of Eqn. 32d for calculation of C_f/C_{fo} results in considerable improvement of agreement between theory and data for this formulation, but only at the expense of worsening agreement between theory and data for the other five formulations. Thus far, no combination of eddy viscosity equations and C_f/C_{fo} expressions considered has resulted in improvement of the predictions for the "problem" formulation without simultaneously degrading the agreement between theory and experiment for the other formulations.

Considerable thought has been devoted to this problem, resulting in definition of an interesting dilemma. Formulation 4525 (73/27 AP/HTPB, 1667°K flame temperature, 20 micron oxidizer) and Formulation 5565 (82/18 AP/HTPB, 2575°K flame temperature, bimodal mix of 90 and 200 micron oxidizer) were tailored to give nearly identical burn rate versus pressure characteristics in the absence of crossflow. This near equality of burning rates resulted from cancellation of a considerably higher temperature driving force ($T_{flame} - T_{surface}$) for the latter formulation by a lower diffusion flame distance associated with the smaller oxidizer formulation. That is, in a no-crossflow situation the diffusion flame zone stretches considerably further from the surface for the 5565 formulation, offsetting the effect of higher flame temperature on burn rate. Thus, it would appear that the heat release zones, being much further out into the higher turbulence (and stronger flame-bending) region of the boundary layer for the 5565 formulation should be much more affected by crossflow for this formulation than for Formulation 4525, and thus the burning rate of 5565 should be much more sensitive to crossflow than that of 4525. Indeed, this is what is predicted by the model and is what it seems to this author must be predicted by any model based on either diffusion-flame bending or turbulence augmentation of transport properties. However, comparison of the data in Figures 8 and 12 reveals that the erosive burning characteristics of these two formulations are essentially identical. This appears to be a fundamental problem for which this author does not currently have an explanation.

Summary

Several variants of a model for the non-erosive burning of unimodal oxidizer composite propellants have been developed. These variants have been tested, with optimization of three "free" constants against no-crossflow burning rate data for a family of four AP/HTPB propellants experimentally studied at Atlantic Research. Three variants, including two which treat the incremental regression of the burning front through an oxidizer crystal and one in which an average-intersection concept is employed, have been found to predict the data quite well. The average-intersection variant was extended to handle crossflows and multimodal oxidizer formulations. This extended model was found to give excellent agreement with no crossflow burning rate data for two additional formulations containing bimodal oxidizer. In the initial development of the erosive burning aspect of the model, columnar diffusion flame bending was assumed to be the only mechanism leading to burn rate augmentation by crossflows. This assumption led to severe underprediction of erosive burning effects, and a flow profile analysis for prediction of turbulence augmentation of transport properties as well as flame-bending was subsequently built into the model. This revised model is found to give good agreement with erosive burning data for five of the six formulations studied, but gives predicted rates higher than observed for the sixth formulation. It is felt that this problem results from an inability to accurately predict turbulence profiles at high blowing ratios (transpiration velocity/crossflow velocity) in combination with the fact that the formulation in question contains very large oxidizer particles, making its predicted burning rate quite sensitive to the boundary layer details.

Nomenclature

AFU	fuel surface area associated with APOX
APOX	planar projection or exposed oxidizer particle surface area
ASOX	total curved oxidizer exposed surface area
B_{sub}	pre-experimental for subsurface reaction rate equation
b	blowing parameter, defined by Eq. 31.
C_f	skin friction coefficient, including transpiration effects
C_{fo}	no-blowing skin friction coefficient
C_p	gas heat capacity
C_{pox}	solid oxidizer heat capacity
D_o	oxidizer particle diameter
DELOX	distance of center of oxidizer crystal surface from initial oxidizer peak
DPOX	diameter corresponding to APOX
$\mathcal{D}$	gas diffusivity (molecular)
$\mathcal{D}_{eff}$	effective total gas diffusivity (molecular plus turbulent)
$E_{ACT,OF}$	activation energy for fuel-oxidizer gas reaction
$E_{ACT,AP}$	acitvation energy for monopropellant oxidizer gas reaction
E_{sub}	activation energy for subsurface reaction
FH90	distance required for mixing of oxidizer and fuel gas streams
h	channel half-height
k	roughness height
K	constant defined by Eq. 34
K_{AP}	constant in expression for oxidizer monopropellant reaction distance
K_{OF}	constant in expression for O/F gas reaction distance
L_{AP}	oxidizer monopropellant gas reaction distance
L_{RX}	oxidizer/fuel gas reaction distance
$M_{crossflow}$	cross flow Mach number (mean)
MW	molecular weight
$\dot{m}_{INJ}$	surface blowing mass flux (burning mass flux based on planar area)
$\dot{m}_{fuel}$	mass flux of fuel
$\dot{m}_{OX,P}$	oxidizer mass flux, based on planar surface projection
$\dot{m}_p$	mass flux of propellant (or subpropellant) based on planar surface area
n	global gas-phase reaction order
P	pressure
R	gas law constant
Re	Reynolds Number based on channel hydraulic diameter
r_{avg}	average linear regression rate of propellant
r_{fuel}	linear regression rate of fuel surface
r_{ox}	linear regression rate of oxidizer, normal to its curved surface
T	temperature
T_{AP}	temperature at location of monopropellant oxidizer flame
T_f	flame temperature
T_{melt}	oxidizer melting temperature
T_c	propellant bulk (initial) temperature
T_s	surface temperature
TAU	time for fuel regression plane to move from one increment to the next
u(y)	crossflow velocity at distance y from the surface
$\bar{U}_{crossflow}$	mean crossflow velocity
U_{fs}	mainstream crossflow velocity
u^*	friction velocity, $U_{fs}\sqrt{C_f/2}$
U_L	defined by Eq. 15
v(y)	transpiration velocity at distance y from the surface
V_{f,d_i}	volume of fuel associated with an oxidizer particle of diameter d_i
$V_{gas,surf}$	gas velocity away from the propellant surface
VLO	volumetric oxidizer fraction in propellant
WFO	weight fraction oxidizer in propellant
XDTOP	distance of fuel surface from initial oxidizer peak
XEXP	exponent used is assignment of fuel to various oxidizer particle size classes
XNA	exponent used in assignment of fuel surface area to various oxidizer-surface intersections (Eq. 18)
y	distance from propellant surface
ZINT	defined by Eq. 14
α	mass fraction of oxidizer reacting at or below propellant surface
	mass fraction oxidizer in overall propellant
γ_i	mass of oxidizer of particle size class i per mass of propellant
γ_i^*	mass fraction oxidizer in subpropellant i
γ_c	specific heat ratio
Δy	offset distance due to roughness (Eq. 41)
ϵ	eddy viscosity
ζ_i^*	volume fraction oxidizer in subpropellant i
λ_{eff}	effective total gas thermal conductivity (molecular plus turbulent)
λ_L	molecular gas thermal conductivity
λ_{ox}	condensed-phase oxidizer thermal conductivity
ϕ	(molar fuel/oxidizer ratio)/stoichiometric fuel/oxidizer ratio)
θ	flow-bending angle (See Fig. 1)
ρ_i^*	density of subpropellant i
ρ_{ox}	oxidizer density
$\rho_{propellant}$	propellant density
ρ_{fuel}	fuel (binder) density
ρ	gas density
ρ_{fs}	mainstream gas density
μ	viscosity (laminar)
$\tau(y)$	shear stress at distance y from the propellant surface
τ_{wall}	wall shear stress
υ	kinematic viscosity, μ/ρ

References

1. King, M., "Effects of Crossflow on Solid Propellant Combustion: Interior Ballistic Design Implications," 1976 JANNAF Propulsion Meeting, Atlanta, Georgia, December, 1976, CPIA Publ. 280, Vol. V, p. 342.

2. King, M., "A Model of the Erosive Burning of Composite Propellants," AIAA/SAE 13th Propulsion Conference, Orlando, Flotida, July, 1977. AIAA Paper 77-930. Also J. Spacecraft and Rockets, 15, 3, May-June, 1978, pp 139-146.

3. King, M., "Erosive Burning of Composite Solid Propellants: Experimental and Modeling Studies," AIAA/SAE 14th Joint Propulsion Conference, Las Vegas, Nevada, July, 1978, AIAA Paper 78-979.

4. King, M., "Erosive Burning of Composite Solid Propellants," 15th JANNAF Combustion Meeting, Newport, R.I., Sept., 1978, CPIA Publ. 297, Vol. II, p. 179-198, Feb., 1979.

5. King, M.K., "Model for Steady State Combustion of Unimodal Composite Solid Propellants," AIAA 16th Aerospace Sciences Meeting, Huntsville, Ala., January, 1978, AIAA Paper No. 78-216.

6. Beckstead, M.W., Derr, R.L., and Price, C.F., "The Combustion of Solid Monopropellants and Composite Propellants," Thirteenth International Symposium on Combustion, The Combustion Institute. Pittsburgh, Pennsylvania. 1971, pp. 1047-1056. Also, "Combustion Tailoring Criteria for Solid Propellants," Lockheed Propulsion Company Report 835F (AFRPL-TR-69-190), May, 1969.

7. Waesche, R.H.W., and Wenograd, J., "Calculation of Solid Propellant Burning Rates from Condensed Phase Decomposition Kinetics," AIAA 7th Aerospace Sciences Meeting, January, 1969, AIAA paper 69-145. Also, United Aircraft Final Report on Research Investigation of the Decomposition of Composite Solid Propellants, Report No. H910457-37, September, 1969.

8. Burke, S.P., and Schumann, T.E.W., "Diffusion Flames," Ind. and Eng. Chem., 20, 10, p. 998, October, 1928.

9. Glick, R.L., and Condon, J.A., "Statistical Analysis of Polydesperse, Heterogeneous Propellant Combustion: Steady-State," 13th JANNAF Combustion Meeting, Monterey, Calif., Sept., 1976, CPIA Publ 281, Vol. II, p. 313, Dec., 1976.

10. Landis, R.B., and Mills, A.F., "The Calculation of Turbulent Boundary Layers with Foreign Gas Injection," Int. J. Heat and Mass Tx, 15, 1905-32, (1972).

11. Kays, W.M., and Moffat, R.J., "The Behavior of Transpired Turbulent Boundary Layers," Report HMT-20, Thermosciences Division, Dept. of Mech. Eng., Stanford Univ., Stanford, Calif., April, 1975.

12. Kays, W.M., "Heat Ttansfer to the Transpired Turbulent Boundary Layer," Int. J. Heat and Mass Tx., 15, 1023-1044, (1972).

13. Schetz, J.A., and Nerney, B., "Turbulent Boundary Layer with Injection and Surface Roughness," AIAA J, 15, 9, p. 1288, Sept., 1977.

14. Mickley, H.S., and Davis, R.S., "Momentum Transfer for Flow Over a Flat Plate with Blowing," NACA Technical Note 4017, November, 1975.

15. Van Driest, E.R., "On Turbulent Flow Near a Wall," Journal of the Aeronautical Sciences, Nov., 1956, p. 1007.

16. Cebeci, T., and Chang, K.C., "Calculation of Incompressible Rough-Wall Boundary-Layer Flows," AIAA Journal, 16, 7, p. 730, July, 1978.

17. Yamada, K., Goto, M., and Ishikawa, N., "Simulative Study on the Erosive Burning of Solid Rocket Motors, AIAA Journal, 14, 9, p. 1170, September, 1976.

18. Liepmann, H.W., "The Rise and Fall of Ideas in Turbulence," American Scientist, 67, March - April, 1979, pp 221-228.

Table I. Unimodal Oxidizer (No Cross Flow) Generation 2 Model Variants Examined

I. ORIGINAL GENERATION 2 MODEL, DESCRIBED IN DETAIL IN REFERENCE 5. UNIFORM DISTRIBUTION OF O/F FLAME HEAT RELEASE BETWEEN X = L_{RX} AND X = L_{RX} + FH90. L_{AP} INDEPENDENT OF LOCAL TEMPERATURE. STEP THROUGH VARIOUS INTERSECTIONS OF OXIDIZER AND FUEL, WITH 3 WAYS OF AVERAGING BURN RATE EMPLOYED.

II. SAME AS I, EXCEPT FOR USE OF AN AVERAGE FUEL-OXIDIZER INTERSECTION CONCEPT.

III. MODIFICATION OF I. ALLOWANCE FOR DEPENDENCE OF L_{AP} ON LOCAL TEMPERATURE. ALTERED DEPENDENCY OF L_{RX} ON T_{flame}. SUBSURFACE HEAT RELEASE CALCULATION MODIFIED TO ALLOW FOR REACTANT DEPLETION. WEIGHTING OF DISTRIBUTION OF O/F FLAME HEAT RELEASE BETWEEN TOP AND BOTTOM OF CONICAL FLAME CHANGED TO BE MORE CONSISTENT WITH DETAILED MIXING PROFILES CALCULATED VIA BURKE-SCHUMANN ANALYSIS.

IV. SAME AS III, EXCEPT FOR USE OF AN AVERAGE FUEL-OXIDIZER INTERSECTION CONCEPT.

V. SAME AS III, EXCEPT FOR ALLOWANCE OF DIFFERENT SURFACE TEMPERATURES FOR BINDER AND OXIDIZER. DIFFUSION FLAME HEIGHTS RELATIVE TO AP SURFACE ADJUSTED TO ALLOW FOR ITS PROJECTION OR DEPRESSION RELATIVE TO BINDER CONTINUUM SURFACE.

VI. SAME AS V, EXCEPT NO ADJUSTMENT OF DIFFUSION FLAME HEIGHTS (WRINKLED FLAME).

IIIA. SAME AS III, EXCEPT THAT FLAME TEMPERATURE IS SET EQUAL TO FLAME TEMPERATURE ASSOCIATED WITH OVERALL COMPOSITION AT ALL INTERSECTIONS.

IIIB. SAME AS III, EXCEPT ASSIGNMENT OF FUEL AREA TO EACH INCREMENTAL INTERSECTION IS DONE VIA $AFU/APOX = C(D_O)^{XNA}$.

IIIC. SAME AS III, EXCEPT O/F RATIO IS FORCED TO BE CONSTANT (AT OVERALL PROPELLANT O/F) AT EACH INTERSECTION BY ADJUSTMENT OF THE ASSOCIATED FUEL AREA AS THE OXIDIZER – SURFACE INTERSECTIONAL AREA CHANGES.

Table II. Propellants Used in Model Checkout.

FORMULATION DESIGNATION	AP/HTPB RATIO	OXIDIZER PARTICLE SIZE (S), MICRONS	THEORETICAL FLAME TEMPERATURE, °K
4525	73/27	20	1667
4685	73/27	5	1667
5051	73/27	200	1667
5542	77/23	20	2065
5565	82/18	13.65% 90 68.35% 200	2575
5555	82/18	41% 1 41% 7	2575

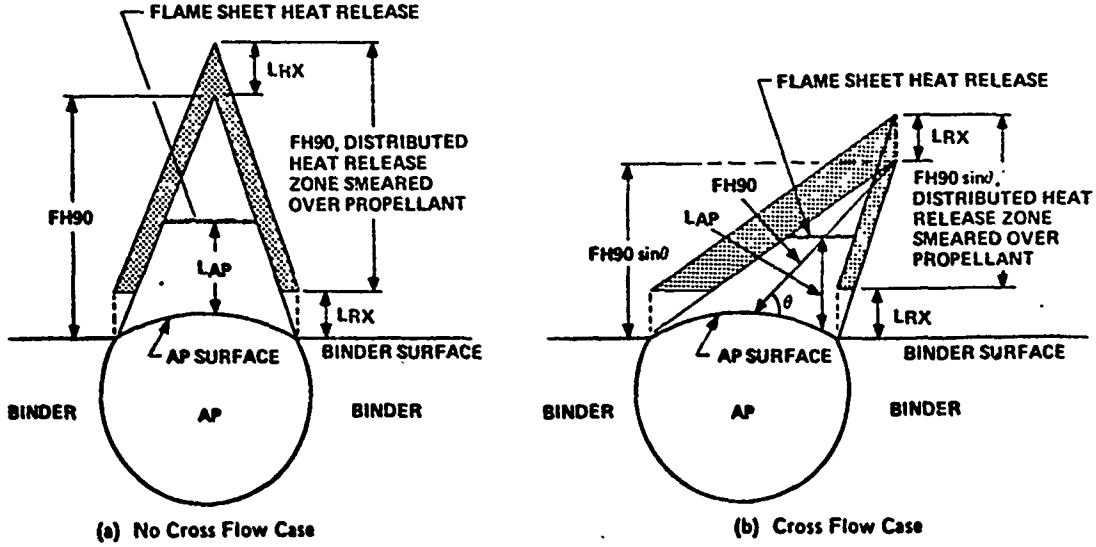

(a) No Cross Flow Case (b) Cross Flow Case

Figure 1. Schematic of Burning Composite Propellant, With and Without Cross Flow

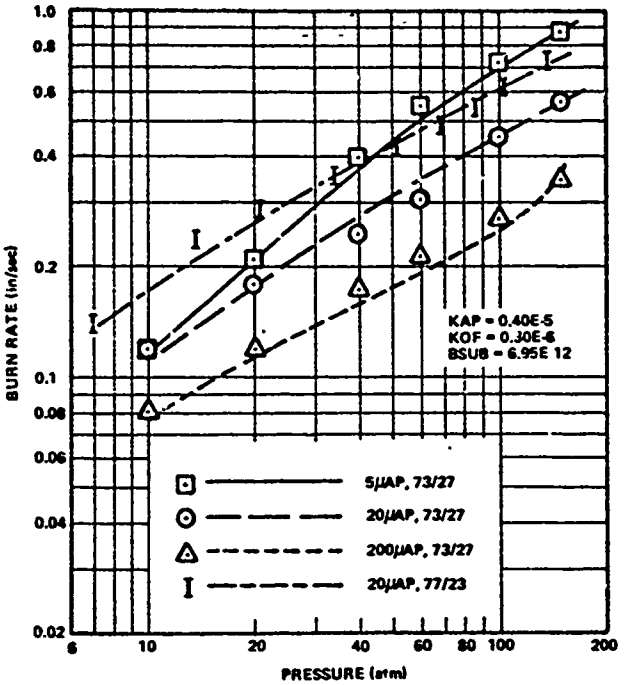

Figure 2. Model Variant IIIA – Theory and Data for Four Unimodal Oxidizer Formulations

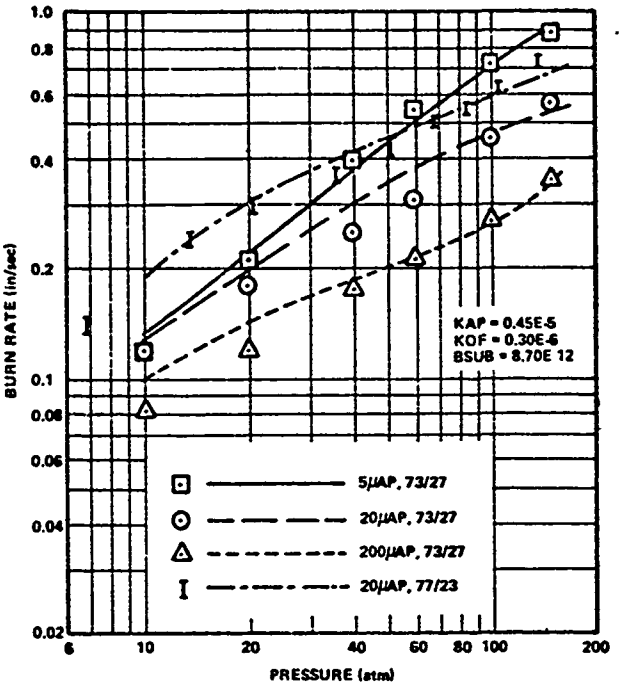

Figure 3. Model Variant IIIC – Theory and Data for Four Unimodal Oxidizer Formulations

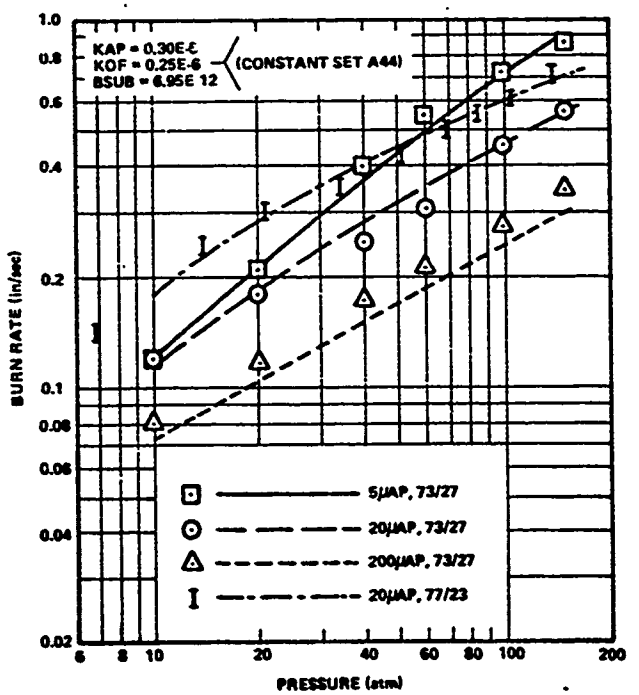

Figure 4. Model Variant IV – Theory and Data for Four Unimodal Oxidizer Formulations

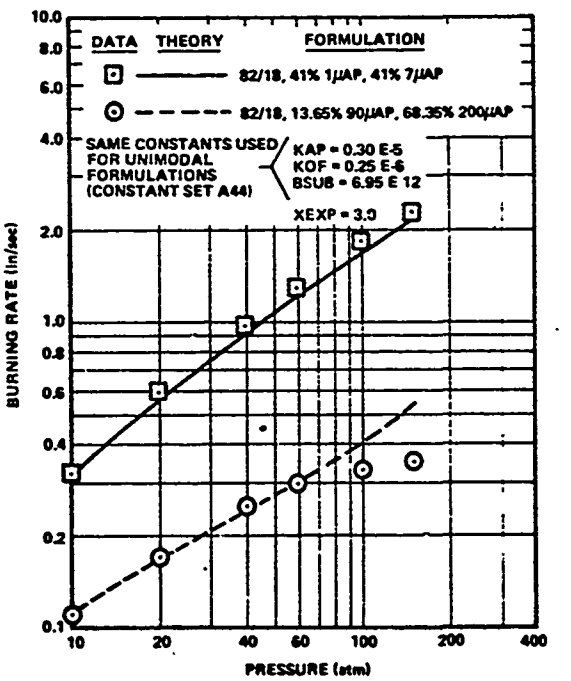

Figure 5. Model Variant IV – Theory and Data for Two Multimodal Formulations

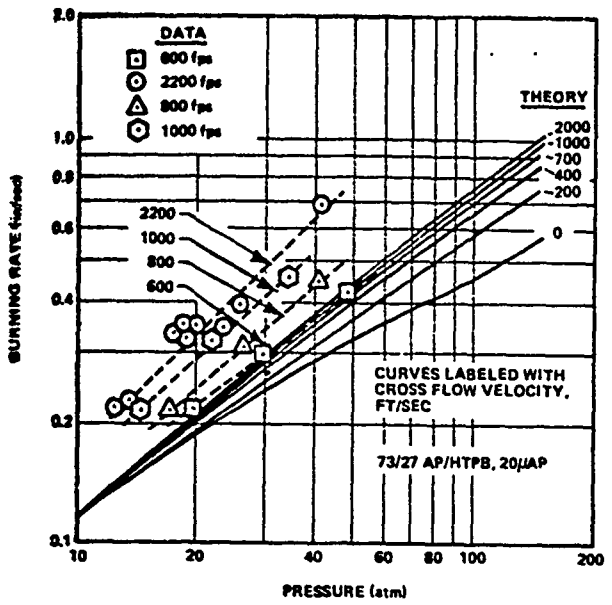

Figure 6. Comparison of Erosive Burning Data with Theoretical Predictions Made Assuming Flame-Bending to be the Only Mechanism Causing Burn Rate Augmentation

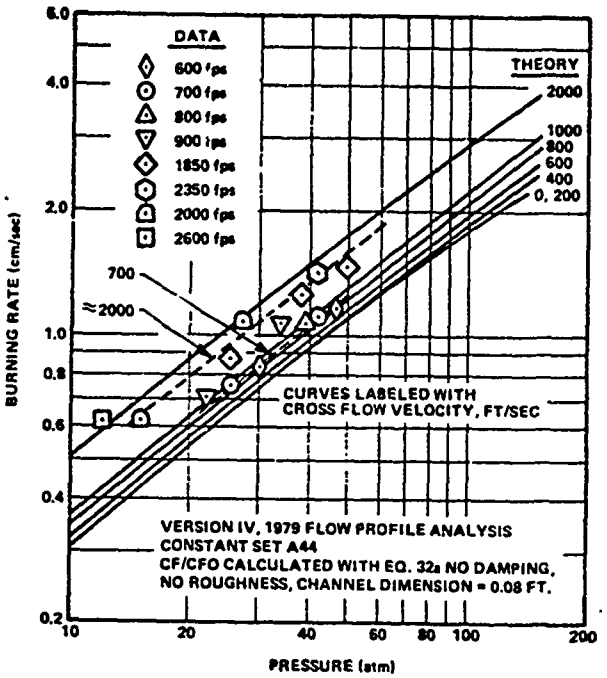

Figure 7. Erosive Burning Data and Predictions – 73/27 AP/HTPB, 5μAP

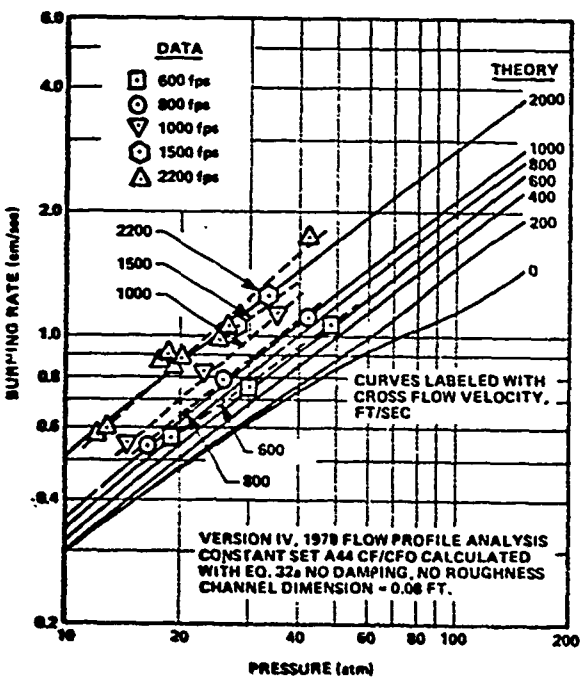

Figure 8. Erosive Burning Data and Predictions – 73/27 AP/HTPB, 20μAP

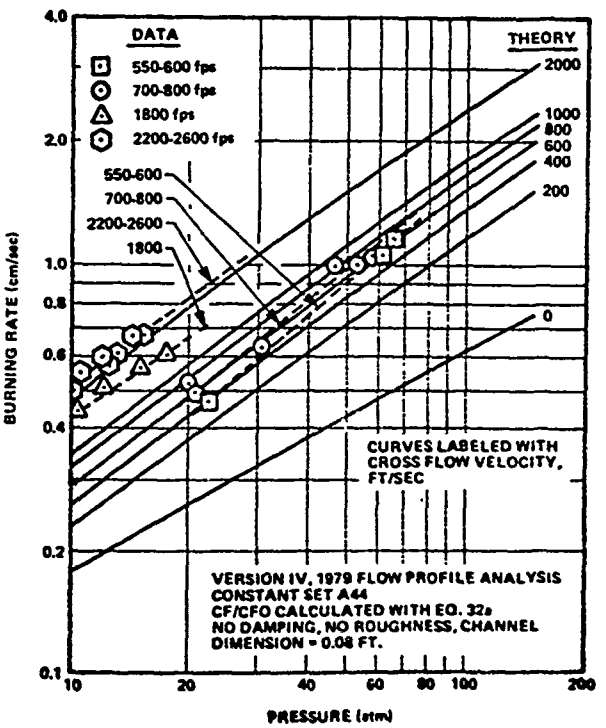

Figure 9. Erosive Burning Data and Predictions – 73/27 AP/HTPB, 200μAP

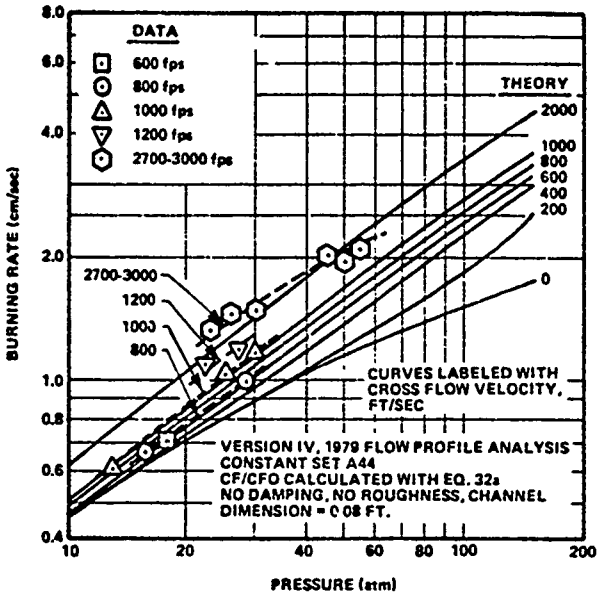

Figure 10. Erosive Burning Data and Predictions - 77/23 AP/HTPB, 20μAP

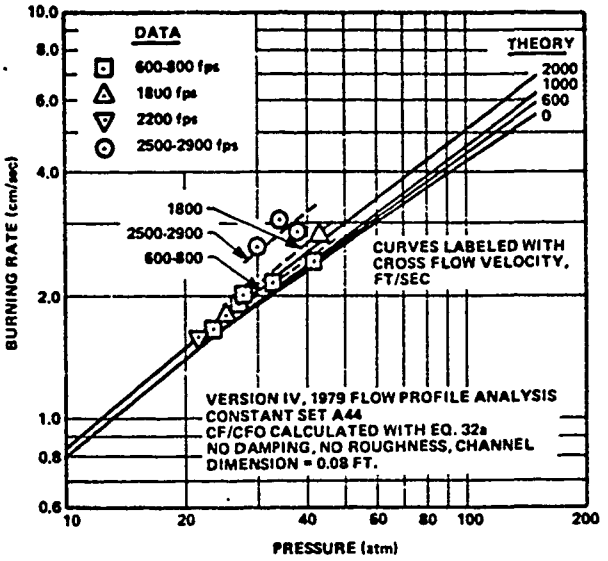

Figure 11. Erosive Burning Data and Predictions - 82/18 AP/HTPB, 41% 1μAP, 41% 7μAP

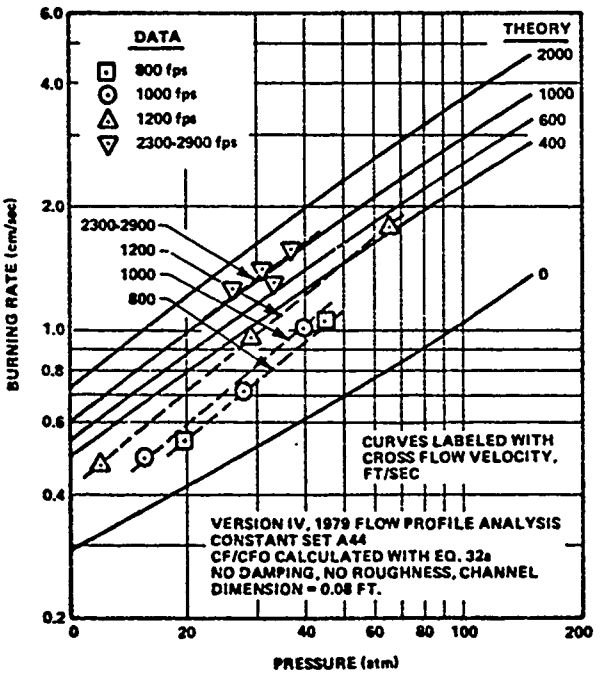

Figure 12. Erosive Burning Data and Predictions - 82/18 AP/HTPB, 13.65% 90μAP, 68.35% 200μAP